Late-kinematic gold mineralisation during regional uplift and the role of nitrogen: an example from the La Codosera area, W. Spain

S. J. Dee and S. Roberts

Department of Geology, The University, Highfield, Southampton SO9 5NH, U.K.

Abstract

Vein formation occurred throughout a deformation sequence which involved early transpressive ductile deformation through to late-kinematic transpressive brittle structures which host a series of gold prospects. Fluid inclusion data from (S1) fabric parallel veins associated with early deformation suggest that a low-salinity aqueous fluid, with a mean salinity of 6.4 wt.%, was present during peak metamorphism. Pelite mineralogy and isochores constrain peak metamorphism to the lowermost part of the upper greenschist facies at 325 to 425 °C and 1.4 to 3.4 kbar.

Fluid inclusion data from auriferous and barren late-kinematic quartz veins, both containing unmixing assemblages of aqueo-carbonic inclusions with low salinities of ≈2.7 wt.% NaCl equiv., indicate unmixing occurred at 300 °C and 1.5 kbar.

Volatiles (CO_2, N_2, CH_4) are observed in all the late-kinematic veins. The N_2 contents of veins with elevated gold grades are typically higher than those with low gold grades. N_2 reaches 8.7 mole% in a vein with 0.49–4.6 p.p.m. Au compared to <1 mole% in a vein with <0.05 p.p.m. Au. The CH_4 content of late kinematic veins is generally less than 1 mole% and shows no relative enrichment in mineralised veins. The generation of N_2 in the mineralising fluid most likely results from interaction of fluid with the ammonium ion, NH_4^+, in micas and feldspars. This interaction could take place either at source, due to metamorphic devolatisation reactions, or along those structures which acted as fluid conduits due to fluid-rock interaction.

Keywords: gold mineralisation, nitrogen, Spain, fluid inclusions.

Introduction

By establishing the vein chronology and fluid chemistry of a mineralised terrane, important constraints can be placed on the timing, source and precipitation mechanisms involved during the mineralising process. This paper describes the fluid chemistry of late-kinematic auriferous quartz veins within part of the Hercynian crust of the Iberian Peninsula around the village of La Codosera, West Spain. Data from early veins associated with the peak metamorphism are compared with those developed during the late-Hercynian fracturing which contain the mineralisation. This enables constraints to be placed on the timing and *P/T* regime of vein formation. In addition, a significant nitrogen anomaly within the mineralised structures is outlined.

The study area lies at the southern margin of the Central Iberian Zone, just to the north of the Badajoz Shear Zone (Fig. 1). The shear zone is a complex structural lineament along which movements were focused during the Hercynian orogeny (Arthaud and Matte, 1974; Lefort and Ribeiro, 1980; Burg *et al.*, 1981) and which played an important role in the amalgamation of Iberian terranes.

A dominantly Precambrian sequence, known locally as the Complejo–Esquisto Grauvaquico (CEG), comprises a monotonous sequence of slates and greywackes which crop out mainly to the north of the La Codosera syncline. A series of Lower Palaeozoic quartzites and slates unconformably overlie the Complejo–Esquisto Grauvaquico and occupy three WNW–ESE trending ridges: the Southern Ridge, which also includes highly sheared Precambrian to Devonian sediments, Central Ridge and Northern Ridge. Between the Central and Southern Ridges lies the La Codosera Syncline cored by Devonian slates,

Mineralogical Magazine, September 1993, Vol. 57, pp. 437–450

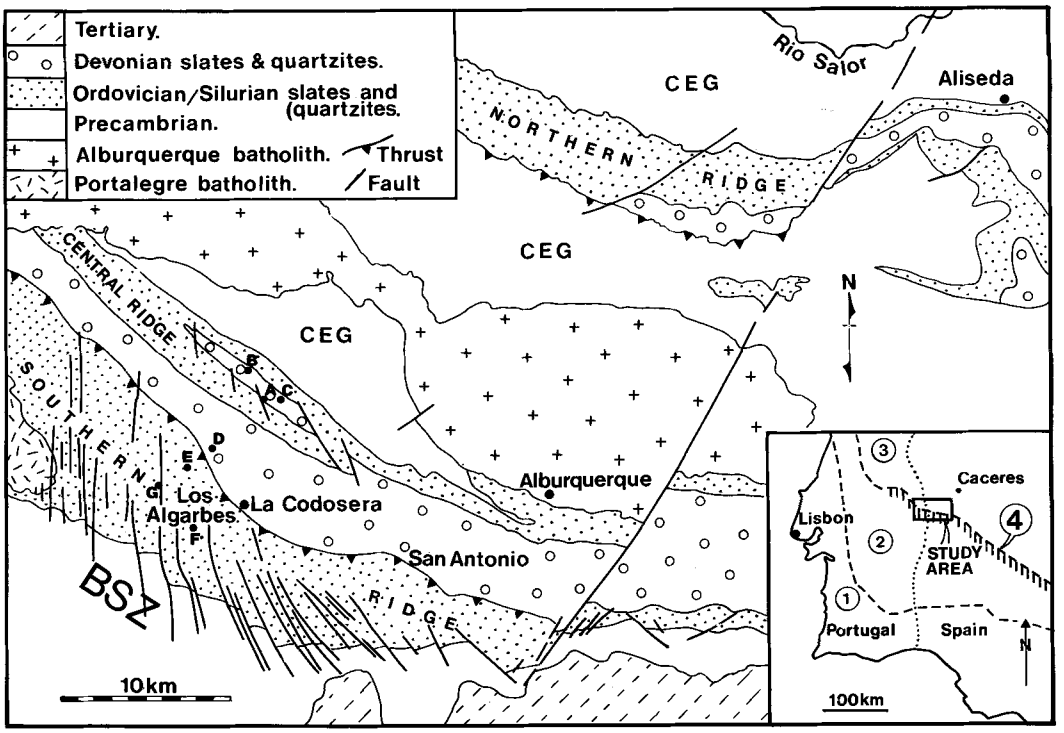

FIG. 1. Location map and geological outline of the La Codosera area. Inset shows the locations of terrain boundaries: South Portuguese Zone (1); Ossa-Morena Zone (2); Central Iberian Zone (3); B.S.Z. Badajoz Shear Zone (4 on inset). Central Ridge Prospects: A = Chirriato; B = Peñon; C = the 100 m E–W Vein. Los Algarbes area prospects: D = Perla de Anibal; E = Portilla Larga; F = Los Algarbes; G = Portilla Arriba.

with some thin sandstone and limestone units (Fig. 1). The late Hercynian Albuquerque batholith is intruded mainly into the CEG but further west, in Portugal, cross-cuts the La Codosera syncline.

Sanderson *et al.* (1991) considered the whole La Codosera area to have been subject to a prolonged period of transpression during the Hercynian orogeny with the greatest strike-slip component localised within the Badajoz shear zone. They recognised early folding and thrusting in response to NE–SW shortening within the Central Iberian Zone, which became increasingly transpressive towards the southern margin. This resulted in a progressive change from thrust to strike-slip tectonics towards the Badajoz–Cordoba shear zone. Late Hercynian fracturing was characterised by a domino style rotation of fault blocks, induced by continued left-lateral transpression (Sanderson *et al.*, op. cit.) (Table 1). The strike of the domino faults rotates progressively counterclockwise towards the east (Fig. 1).

The most significant gold prospects of the area are related to the late Hercynian domino-style faulting described by Sanderson *et al.* (op. cit.). The geographical location of the Au veins, within the Central Ridge and the Los Algarbes area of the Southern Ridge, are indicated on the location map (Fig. 1). Individual prospects are described in Table 2. The principle sulphide assemblage within the veins is pyrite and arsenopyrite with gold occurring principally within arsenopyrite and pyrite. Visible gold is rarely seen. Three styles of mineralised vein occur (Roberts *et al.*, 1991) which post-date the early ductile deformation in the area (Table 1):

(i) High-angle veins—a series of milky quartz veins which trend between 020° to 060°;
(ii) Strike fault-related prospects—these veins occur along small detachment surfaces parallel to strike which dip gently to the SW and show oblique–reverse separation (oblique thrusts);
(iii) East–west-trending veins—within the core of the Central Ridge anticline a series of east–west trending quartz veins are developed, forming an *en echelon* array with a sinistral sense of shear.

Table 1. Deformation chronology in the La Codosera area.

Age	Structure	Symbol
Late Hercynian.	Brittle transpressive deformation with a left lateral component leading to domino-style rotation of fault blocks and extensive late faulting and fracturing. Gold mineralisation associated with this deformation.	
	Regional kink bands and late cleavages.	**KB, S_3 & S_4**
D2 Early Hercynian. (2nd Phase)	Asymmetric folding with sinistral / northerly vergence.	**F_2**
	Crenulation cleavage associated with F_2 folds.	**S_2**
	Thrusting with northerly-directed reverse separation and oblique left-lateral movement.	**T_2**
D1 Early Hercynian. (1st Phase)	Steeply-inclined, sub-horizontal folds.	**F_1**
	Steep slaty cleavage (Main Hercynian cleavage).	**S_1**
	Original bedding foliation.	**S_0**

The obliquely reactivated thrusts and high-angle faults appear to accommodate the bulk transpressive strain within the zone and their contemporaneity (Dee, 1992) suggests that the late-brittle transpressive deformation is the fundamental control on the localisation of the mineralisation. The major series of prospects within the Los Algarbes area is located in the region where late domino faulting changes from low-displacement N–S to high-displacement NW–SE orientations (Roberts *et al.*, 1991). This indicates the fundamental control of these large faults on the localisation of the mineralisation.

Analytical techniques

Microthermometric analyses were performed on polished wafers using a LINKAM THM600 heating-freezing stage (Shepherd, 1981). Calibration was performed using a synthetic fluid inclusion standard and chemical standards (as outlined in Shepherd *et al.*, 1985), and performance was monitored using an internal standard. Accuracy is calibration-dependent and is estimated at ±0.5 °C between −60 and −20 °C, ±0.2 °C between −20 and 30 °C, ±1 °C between 30 and 200 °C and +5 °C between 200 and 500 °C. The precision of the instrument is ±0.2 °C for clearly observed phase changes.

Raman analyses were completed on a Jobin Raman Microprobe MOLE S3000 fitted with an Astromed CCD Multichannel detector cooled to 132 °K. Typical integration times were 600 seconds with a single readout. The exciting radiation used the 514.5 nm (green line) of a Coherent 4W Argon laser with a typical source output of 600 mw. Molar calculations were derived using the cross-sections and equations of Dubessy *et al.* (1982) and Romboz *et al.* (1985) respectively. Nitrogen scattering was verified by recording host mineral spectra under the same operating conditions.

Constraints on peak metamorphic conditions

Low-grade regional metamorphism of the pelites, coincident with S1 fabric development, yielded an assemblage of quartz–chlorite–muscovite–albite–(±K-feldspar ± dolomite), typical of the lower greenschist facies. Incipient biotite is developed within microfold hinges related to the primary phase of folding D1 and within porphyr-

Table 2. Description of the mineralised prospects studied.

Prospect (Sample)	Structural Setting and Timing	Vein Length	Vein Width	Au Grade (gt^{-1})
Central Ridge				
Chirriato (1076)	Extension vein due to sinistral shear on the Central Ridge.	100m minimum, possibly > 200m.	0.6m	0.96-5.1
Peñon (289:001 & 289:007)	Reactivated strike-parallel thrust.	180m	0.4m	0.05-1.15
100m E-W Vein (289:056)	Extension vein due to sinistral shear on the Central Ridge.	95m	0.5m (quartzite) 1.5m (slate)	0.49-4.6
Los Algarbes Area				
Perla de Anibal (289:173)	Late high-angle faulting.	45m minimum	0.05-0.25m	0.15-7.2
Portilla Larga (289:010)	Late high-angle faulting.	50m	1m maximum.	0.09-22.8
Los Algarbes (390:006, 390:007 & 289:236)	Reactivated strike-parallel thrust and late high-angle faulting.	detachments 1-5m	detachments 0.05-0.5m	0.11-3.7
Portilla Arriba (289:235)	Reactivated strike-parallel thrust and late high-angle faulting.	detachments 1m	detachments 0.1m	1.2-26.7

oblasts parallel to S1 cleavage. XRD analyses indicate that 2M-micas are present which constrains the lower thermal limit to 280 °C, above the illite field (Hoffman and Hower, 1979). Biotite forms an upper thermal limit at between 400 and 425 °C (Nitsch, 1970), marking the transition from lower to upper greenschist facies. Vitrinite reflectance data from organic matter in the pelites show an Rv_{MEAN} of 5.5% (Dee, 1992) with a resulting temperature estimate of 325 °C (Barker and Pawlewicz, 1986) or 410 °C using the temperature index of Price (1983).

These data combine to delineate a temperature window for the metamorphism of between 325 °C and 425 °C (Fig. 2). The coincidence of the vitrinite geothermometer of Price (1983) and the onset of biotite formation suggests that the true peak conditions are towards the higher end of the indicated temperature range.

To constrain the *P–T* regime of the peak metamorphism, fluid inclusions from early veins were studied. These veins relate to the 1st phase of Hercynian deformation and the veins parallel the S_1 fabric. A population of two-phase (L_{H_2O} + V) inclusions (E_{FP1}) occur within short trails which terminate on crystal boundaries, and as isolated clusters or spaced trails parallel to solid wallrock inclusion bands. These are interpreted as a primary population related to vein growth by a crack-seal mechanism (Fig. 3). A second type of inclusion, E_{FP2}, occurs along grain boundaries

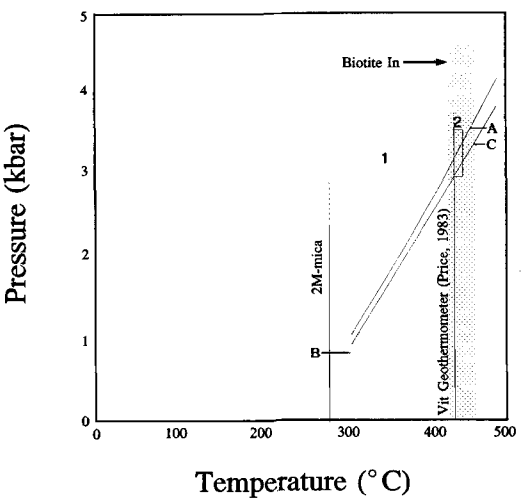

FIG. 2. *P–T* bivariate plot showing the positions of the relative geothermometers and isochores constructed for early fluid inclusions. 1. *P–T* field defined by the vitrinite geothermometers. 2. *P–T* field defined by the Price (1983) vitrinite geothermometer and the incoming of biotite. Isochore A is for the system H_2O–NaCl and isochores B and C are for the system H_2O–CO_2–NaCl (1 and 5 mole% CO_2 respectively).

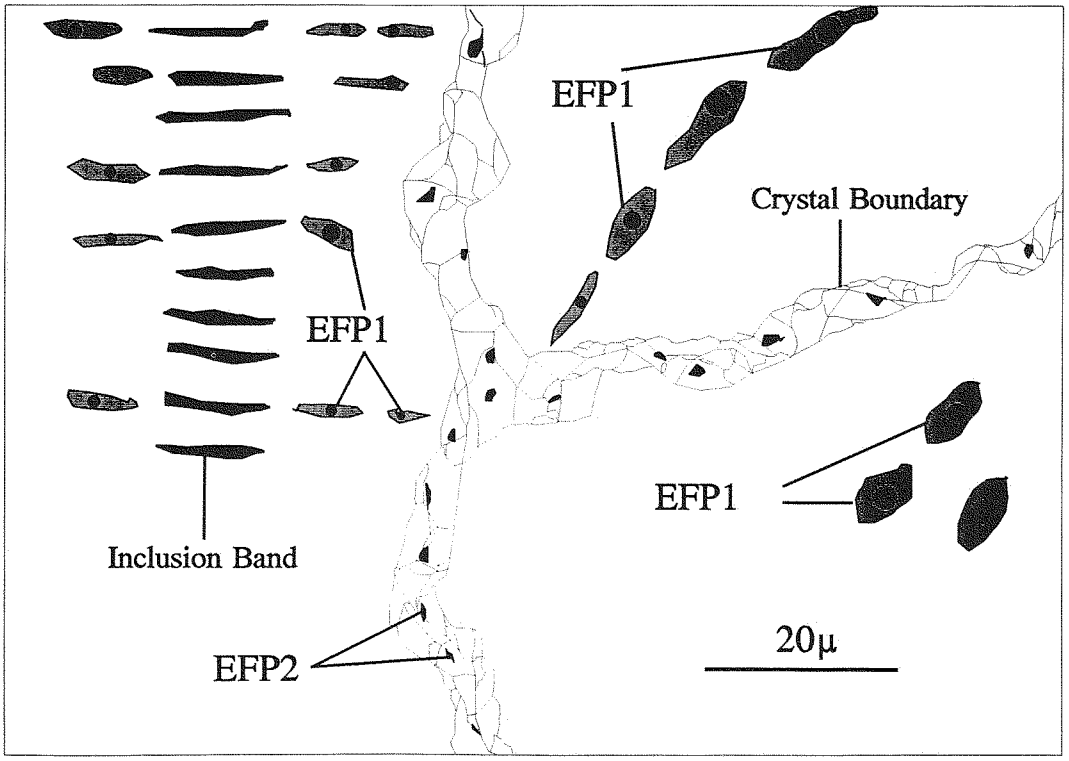

FIG. 3. Schematic illustration of inclusions from fabric-parallel veins. E_{FP_1} inclusions occur as short trails terminating at crystal boundaries, as small isolated clusters or parallel to inclusion bands indicating vein growth by crack-seal mechanisms. E_{FP_2} inclusions are small, and occur along grain boundaries associated with the development of subgrains.

where crystal plastic deformation and recovery have led to recrystallisation of the quartz. E_{FP2} inclusions are too small for microthermometric analysis and their compositions are unknown.

E_{FP1} inclusions show a degree of fill (volume of liquid estimated by comparison with standard volumetric charts, Shepherd *et al.*, 1985) between 0.7 and 0.95 with a mean value of 0.87 and a standard deviation of 0.05 (Fig. 4A). During freezing–warming runs, ice melting (Tmlce) varied between −2 and −7 °C. A frequency histogram of salinity, based on the data regression of Potter *et al.* (1978), shows a positively skewed salinity with a mean value of 6.4 wt.% NaCl equiv. (Fig. 4B). Eutectic melting around −21 °C was observed in some inclusions, indicating NaCl is probably the dominant dissolved salt. Some inclusions developed clathrate on cooling which melted between 4 and 9.1 °C. This indicates the presence of a minor component of $CO_2(\pm CH_4 \pm N_2)$.

On heating, the inclusions homogenise by the disappearance of the vapour bubble ($L + V \rightarrow L$). The recorded temperatures of total homogenisation (ThTOT) show a normal distribution with a mean value of 220 °C (Fig. 4C). The tightly defined range of temperatures of total homogenisation (ThTOT) for E_{FP1} inclusions suggests that they represent a single fluid population.

Isochores were calculated with the equations of Zhang and Frantz (1987) for the system H_2O–NaCl and Brown and Lamb (1989) for the system H_2O–CO_2–NaCl; these equations are incorporated in a computer program FLINCOR (Brown, 1989). Isochore A shows the calculated isochore for E_{FP1} inclusions (Fig. 2). Addition of small amounts of CO_2, modelled using the Brown and Lamb (1989) equation—1 mole% CO_2 for isochore B and 5 mole% CO_2 for isochore C (Fig. 2)—indicates that isochores are shifted to lower pressures, at a given temperature, with increased CO_2. However, these shifts are minimal with respect to the uncertainties constraining the peak metamorphic temperature.

Combination of the petrographic and microthermometric data enables *P–T* estimates to be

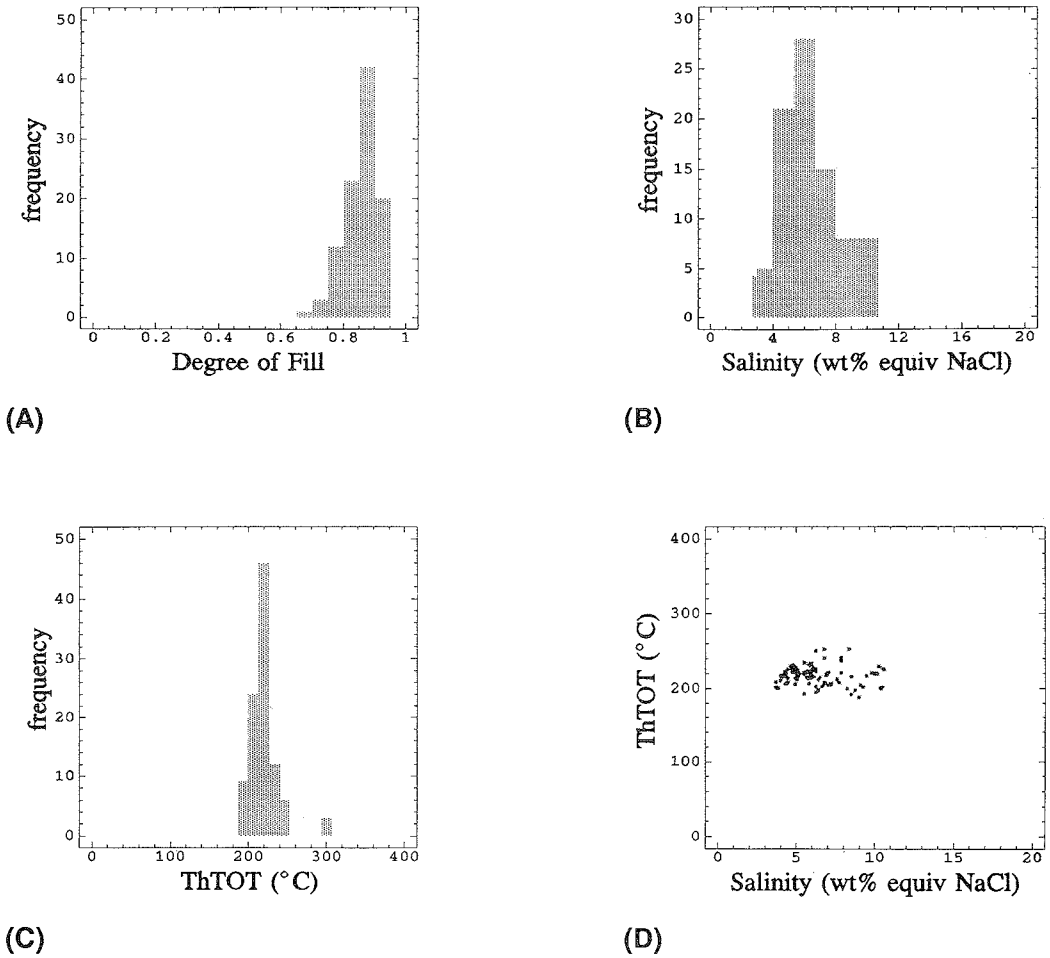

FIG. 4. Microthermometric data E_{FP} inclusions: (A) Degree of fill (n = 101); (B) Salinity (wt.% equiv. NaCl; n = 85); (C) ThTOT (°C; 101); (D) Salinity *vs.* ThTOT (n = 85).

made. The field defined by the vitrinite geothermometers (Dee, 1992) provides a wide estimate of 325 °C to 410 °C, 1.4 kbar to 3.1 kbar. A temperature range based on the coincidence of incipient biotite formation and the Price (1983) geothermometer of 410–425 °C yields pressure estimates of 3.1 kbar to 3.4 kbar. This is the maximum *P–T* estimate that is used in the following sections.

Fluid characteristics of the late kinematic veins

Fluid inclusions have also been studied from a variety of late-kinematic veins which post-date the main S1 fabric and often show sulphide and gold mineralisation (Roberts *et al.*, 1991). Veins sampled from the mineralised prospects are outlined in Table 2. Fluid inclusions from these samples were studied in quartz with simple interlocking textures and with primary sulphide minerals (pyrite and arsenopyrite).

In addition, barren late veins associated with the late domino faults were studied: 1SD5 and 1SD19 from 040° trending faults; 1SD18 from an 048° trending fracture; 1014c and 1014r from a 034° trending sinistral *en echelon* array. Fluid inclusions were studied in fibrous and drusy quartz from these veins.

The most abundant inclusion types within late vein samples (L_{AC}) contain 3 phases at room temperature (L_{H_2O} + L_{CO_2} + V) and occur as discrete inclusions in clusters or in short trails which show negative crystal to irregular shapes.

The optical characteristics of these late inclusions are summarised in Fig. 5. These inclusions are interpreted as primary and representative of the fluid present at the time of vein formation. A second two phase aqueous inclusion population (L_{A1}) is observed and is restricted to trails which clearly post-date the aqueo-carbonic inclusions. In two samples, these inclusions coexist with monophase carbonic inclusions (L_C) suggesting possibly that fluid immiscibility occurred at a late stage within the vein system (Dee, 1992).

The degree of fill of the L_{AC} aqueo-carbonic inclusions (defined here as the relative volume of the aqueous phase measured at the homogenisation temperature of CO_2) varies from <0.2 to 0.9 (Fig. 6A). During freezing–warming cycles the carbonic phase in the inclusions freezes at around −120 °C and, on heating, melting of the solid CO_2 occurs between −61 and −56.6 °C (Fig. 6B). Inclusions were held a few degrees below their melting temperatures to allow the solid CO_2 to form a single solid mass. There is often a temperature interval of around 0.2 °C over which CO_2 melts, indicative of additional volatile components.

Ice melting is difficult to observe in these inclusions and the next reported phase change, clathrate melting, occurs between 5.5 to 12 °C (Fig. 6C). Clathrate decomposition temperatures of >10 °C, $TmCO_2$ values below −56.6 °C and melting of solid CO_2 over a temperature interval, all indicate the presence of additional volatiles. An average salinity for the inclusions has been calculated from the data for all inclusions which appeared to be representative of the system H_2O–CO_2–NaCl (i.e. inclusions whose $TmCO_2$ was close to that for pure CO_2 at −56.6 °C). A mean clathrate melting temperature of 8.6 °C yields a value of 2.7 wt.% NaCl equiv. Carbonic homogenisation of the liquid, vapour or critical states occurs in the temperature range 15 to 31.1 °C (Fig. 6D). This phase transition always occurs above the temperature of clathrate melting and the measured density of the carbonic phase (from $ThCO_2$) is not affected by the retention of CO_2 in clathrates.

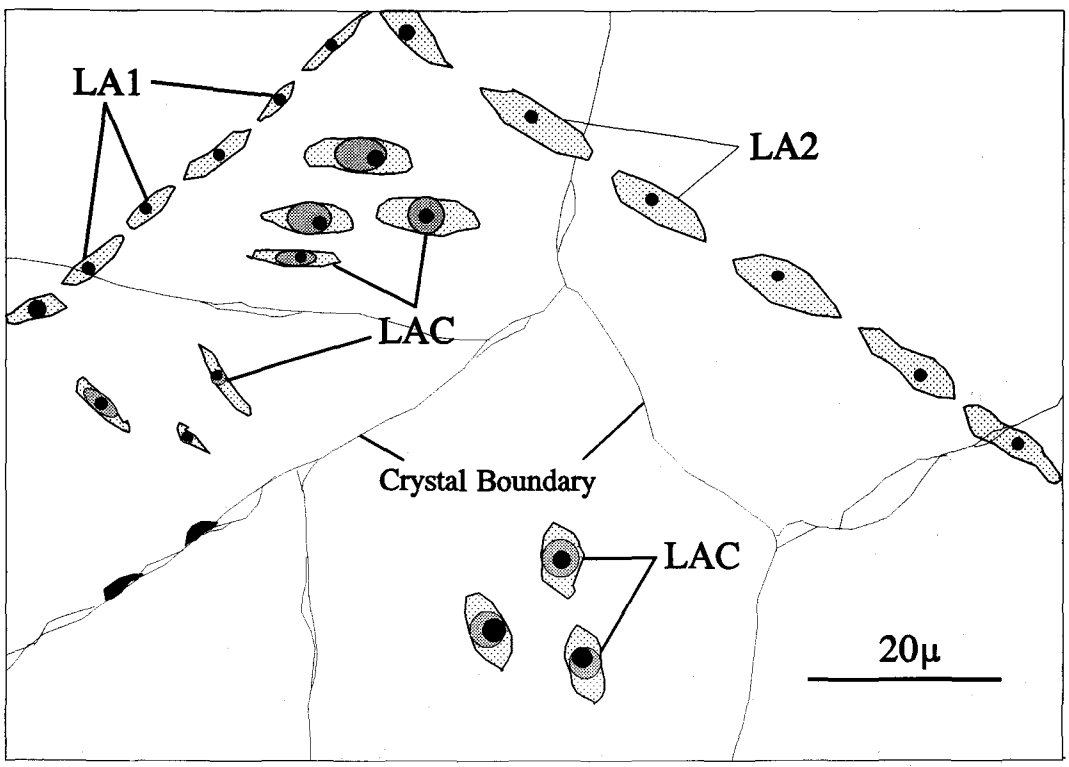

FIG. 5. Schematic illustration of inclusions from late veins. Aqueous L_{A1} inclusions occur in secondary trails which cross-cut crystal boundaries. Aqueo-carbonic L_{AC} inclusions, of differing degrees of fill, co-exist within small clusters. Aqueous L_{A2} inclusions occur as late trails which cross-cut crystal boundaries.

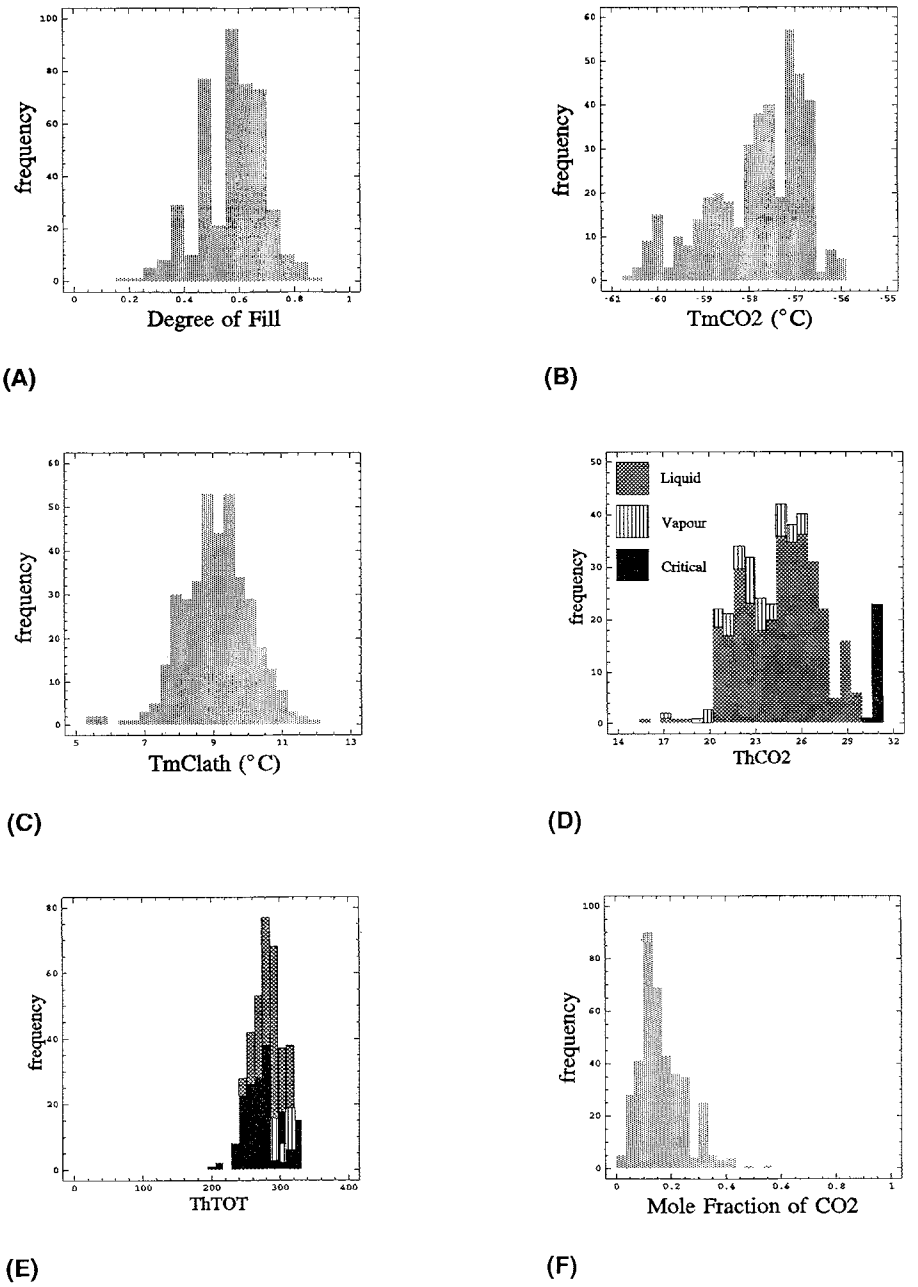

FIG. 6. Summary plots for all 3 phase carbonic (L_{AC}) inclusions: (A) histogram of the degree of fill (n = 439); (B) histogram of $TmCO_2$ (°C; n = 419); (C) histogram of TmCLATH (°C; n = 362); (D) histogram of $ThCO_2$ (°C; n = 391); (E) histogram of ThTOT (°C; 388); (F) histogram of the mole fraction of CO_2 (n = 390).

Total homogenisation occurs to the liquid, vapour and critical states. Decrepitation of inclusions is common and partial decrepitation may be recognised by a change in the degree of fill following an homogenisation run. The temperature of total homogenisation (ThTOT) varies from 200 to 335 °C with a clearly defined peak at 290 °C (Fig. 6E).

The degree of fill varies with the mode of total homogenisation and corresponds to the different amounts of CO_2 present within the inclusion. Inclusions which homogenise to the vapour state ($L_{CO_2} + L_{H_2O} \rightarrow L_{CO_2}$) have a $X_{CO_2} > 0.25$, to the liquid state ($L_{CO_2} + L_{H_2O} \rightarrow L_{H_2O}$)$X_{CO_2} \approx 0.15$ and those inclusions which homogenise critically ($L_{CO_2} + L_{H_2O} \rightarrow C$) have a $X_{CO_2} \approx 0.2$ (Fig. 7). The similar total homogenisation temperatures for the aqueous-carbonic inclusions, despite their differing mode of occurrence and the co-existence of the variable inclusion types, is consistent with the trapping of a fluid at a solvus, with critical total homogenisation (ThTOT → Critical) corresponding to the top of the solvus. Comparison of the data set with the *T*–X sections of Bowers and Helgeson (1983) indicates that the data set are consistent with the unmixing of a low salinity fluid (2.7 wt.% equiv. NaCl) (Fig. 7). However, addition of $N_2 + CH_4$ probably changes the position of the solvus.

The combined petrographic and fluid inclusion data from the pelitic host rocks and early veins, in association with data from the late kinematic veins, allow the *P–T* evolution of the area to be constrained. Peak metamorphism occurred around 3.1 to 3.4 kbar and 410–425 °C, giving a maximum burial of *c.* 12.5 km. The late kinematic veins were developed post-peak metamorphism during uplift. The unmixing H_2O–CO_2 fluid inclusion population indicates fluid entrapment at 1.5 kbar and 300 °C at a level of <6 km in the crust. These values are in accord with the post-kinematic setting of auriferous veins in mesothermal gold systems, commonly observed in metamorphic and mineralised terranes (Groves and Foster, 1991; Nesbitt, 1991). This pressure–temperature–time evolution for the La Codosera area is illustrated in Fig. 8.

Additional volatiles in barren and mineralised late veins

The aqueo-carbonic inclusions of the late-kinematic veins show evidence of unmixing. The $TmCO_2$ values are often depressed below −56.6 °C, with the mineralised late-kinematic veins in particular showing significant depressions in $TmCO_2$ (Fig. 9A). The volatile composition of fluid inclusions from four samples of late-kinematic veins were determined by laser Raman spectroscopy. The samples from the mineralised localities are described in Table 2. Two samples (samples 1076 and 289:056) were from prospects where reported gold grades range from 0.96 to 5.1 p.p.m. One sample was from a poorly mineralised prospect where the gold grade ranges from 0.05 to 1.15 p.p.m. Au (Sample 001). A fourth sample was from a barren vein with <0.05 p.p.m. Au (Sample 1014C). The data are presented in Table 3 and are summarised in a ternary CO_2–N_2–CH_4 plot (Fig. 9).

The volatile phase in all samples is dominantly CO_2 (volatile mole fraction of CO_2, $Z_{CO_2} > 0.80$)

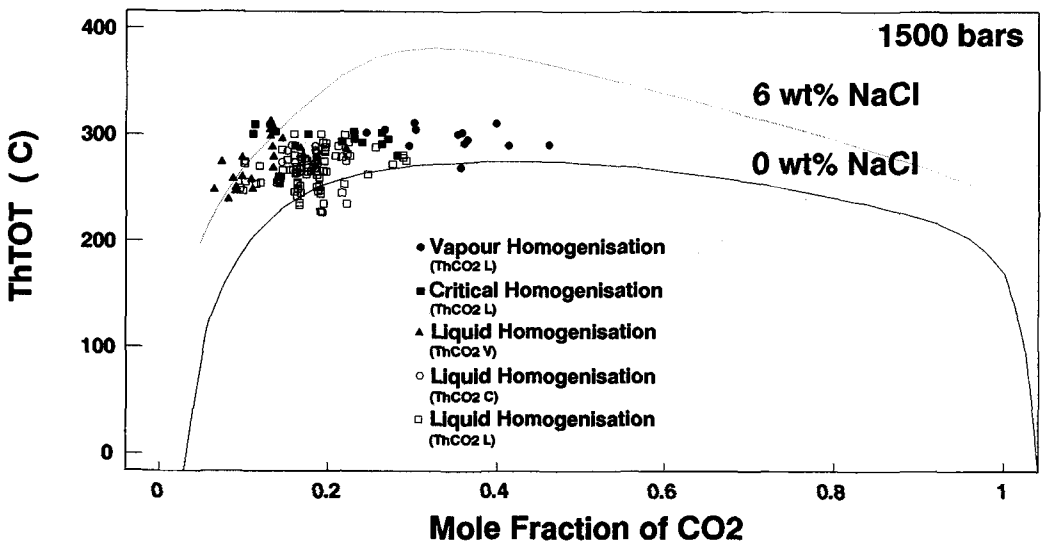

FIG. 7. T–X_{CO_2} plot for the system H_2O–CO_2–NaCl showing the modes of homogenisation ($ThCO_2$ and ThTOT) of the late aqueo-carbonic (L_{AC}) inclusions. The positions of the solvus for 0 and 6 wt.% NaCl at a pressure of 1500 bars (from the data of Bowers and Helgeson, 1983) are also plotted. The range of data for L_{AC} inclusions for and average salinity of 2.7 wt.% NaCl equivalent, fits the theoretical solvus well.

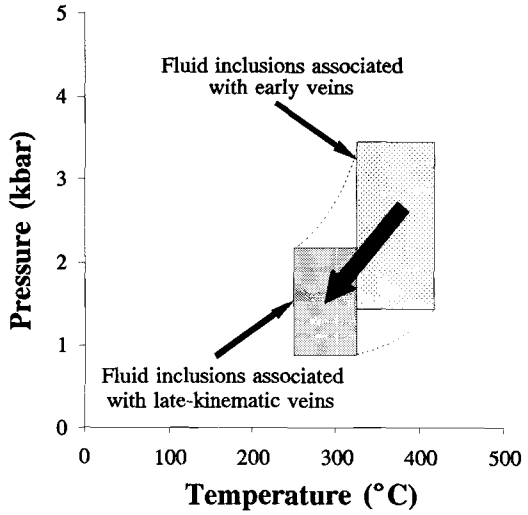

FIG. 8. Pressure–temperature evolution of the area showing the evolution from early veins associated with peak metamorphism through to late kinematic veins which host the gold mineralisation.

in all cases, with variable amounts of N_2 and CH_4. The additional volatile constituents, in particular N_2, clearly increase from the barren vein (1014c; Z_{N_2} 0.02–0.06) through the weakly mineralised vein, 289:001, to the mineralised samples 1076 and 289:056 (Z_{N_2} 0.14–0.17) (Fig. 9B). The increase in additional volatiles is apparently restricted to N_2 with the CH_4 values remaining more or less constant ($Z_{CH_4} \approx 0.01$). In terms of the total inclusion, N_2 reaches 8.7 mole% (or Z_{N_2} of 0.17) in mineralised veins and compares with values of $X_{N_2} < 1$ mole% in barren veins.

Examination of the microthermometric characteristics of inclusions within late-kinematic veins shows that the highest concentrations of N_2 are within inclusions with $ThCO_2 \rightarrow L$ and $ThTOT \rightarrow V$ ($Z_{N_2} \approx 0.140$ to 0.172) and the lowest within inclusions with $ThCO_2 \rightarrow L$ and $ThTOT \rightarrow L$ ($Z_{N_2} \approx 0.018$ to 0.060). Inclusions with $ThCO_2 \rightarrow V$ & $ThTOT \rightarrow L$ have an intermediate concentration of N_2 ($Z_{N_2} \approx 0.030$ to 0.116). As noted earlier, mineralised veins generally show greater depressions in $TmCO_2$ than non-mineralised veins (Fig. 9A). This is consistent with the observation of inclusion abundances within the samples. Samples with elevated gold grades contain a greater abundance of inclusions with $ThCO_2 \rightarrow L$ and $ThTOT \rightarrow V$.

Discussion

Origin of anomalous nitrogen in mineralised veins. All the aqueo-carbonic inclusions from the late-kinematic veins contain measurable quantities of nitrogen, and clearly, inclusion populations from both the mineralised and barren veins contain a nitrogen signature.

Pelitic schists are the dominant lithology of the La Codosera area. Micas in pelitic rocks can contain over 2000 p.p.m. NH_4^+ which can be released into a fluid during prograde metamorphism (Halam and Eugster, 1976). The nitrogen is probably of biogenic origin which, during diagenesis and metamorphism, is stored as the ammonium ion, NH_4^+, within phyllosilicates or feldspars (substituting for K^+ in muscovite and Na^+ in albite, for example). Indeed, NH_4^+ abundances were found to decrease with increasing metamorphic grade in the Dome de L'Agout, France (Duit *et al.*, 1986), accounting for the high N_2 content observed in the fluid inclusions of the area. Isotopic data for N_2, fixed as NH_4^+ in metamorphic rocks, can increase from mean $\delta^{15}N$ values of +5.3‰ in low grade rocks to +9.6‰ in high-grade rocks (Haendel *et al.*, 1979). This fractionation was interpreted either as evidence for exchange reactions or kinetically controlled N_2 loss with increasing temperature.

A correlation between the N_2/CO_2 ratio of fluid inclusions in gold-bearing quartz veins and the style of the mineralisation in the Escadia Grande schist terrain of northern Portugal was described by Naden and Shepherd (1991). Fluids derived within the schists are characterised by high N_2/CH_4 ratios, whereas in the Jales grante terrain the veins are characterised by low N_2/CH_4 ratios. These data are consistent with the production of N_2 from NH_4^+ within the schists, as granites are characterised by relatively low NH_4^+ contents and pelites by relatively high NH_4^+ contents.

Wilkinson (1991) monitored the C–O–H–N–S mass balance of pelites during contact metamorphism in SW England and demonstrated that, given fluid–rock interaction and concomitant loss of nitrogen from the pelites to the fluid, the predicted metamorphic fluid composition showed remarkable similarities to the observed fluids trapped in fluid inclusions in syn-granite metamorphic aureole veins. Bottrell *et al.* (1988*a*,*b*) calculated that nitrogen, trapped in fluid inclusions in quartz veins from the Llanbedr formation North Wales, was released into the fluid during metamorphism of a dominantly pelitic assemblage.

These data tend to support the generation of N_2 into metamorphic fluids by fluid–rock interaction within pelitic lithologies according to:

$$K^+_{(aq)} + NH_4\text{-mica} \rightleftharpoons NH^+_{4(aq)} + K\text{-mica}. \quad (1)$$

Reaction of the ammonium ion, NH_4^+ and fluid,

decreases the pH of the fluid and consumes O_2, thus acting as a powerful reducing agent according to the reactions:

$$NH^+_{4(aq)} + OH^-_{(aq)} \rightleftharpoons NH_{3(aq)} + H_2O_{(l)} \quad (2)$$

$$4NH_3 + 3O_2 \rightleftharpoons 2N_2 + 6H_2O. \quad (3)$$

The lack of thermodynamic data precludes detailed modelling of the effects of N_2 produced by fluid–rock interaction, on gold solubility. However, a decrease in pH would decrease the solubility of a AuHS° complex (Seward, 1989) but increase the solubility of chloride complexes.

The data presented show that veins with enhanced gold-grades correlate with increased levels of N_2 within fluid inclusions. A viable mechanism for the production of N_2 in the mineralised veins from the La Codosera area is fluid–rock interaction with the concomitant reduction of the fluid promoting gold deposition. This could explain the association of N_2 and enhanced gold grades within late-kinematic post-peak metamorphic veins.

One problem with this model is why the late-kinematic fluids are enriched in N_2, CO_2 and Au

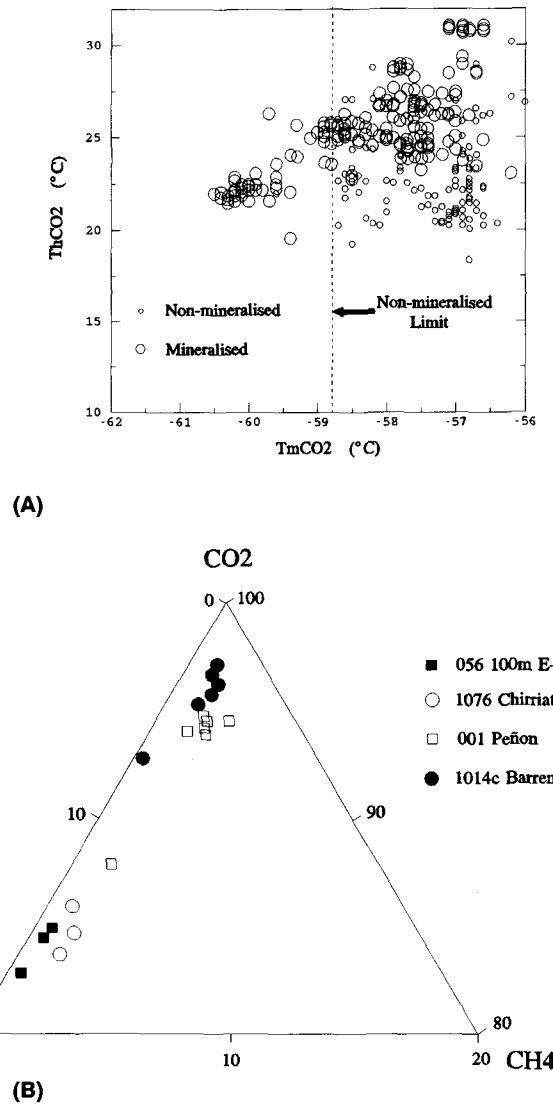

FIG. 9. (A) $TmCO_2$ *vs.* $ThCO_2$ for the aqueo-carbonic inclusions from mineralised and non-mineralised veins. (B) Triangular plot of N_2–CH_4–CO_2 for the aqueo-carbonic inclusions. Mineralised veins have higher Z_{N_2}.

Table 3. Raman analyses of L_{AC} inclusions. Data are presented as mole fractions of the volatile phase (eg. Z_{N2}) and as mole fractions for the whole inclusion (eg. X_{CO2}).

Sample	Type	Z_{CO2}	Z_{N2}	Z_{CH4}	X_{H2O}	X_{CO2}	X_{N2}	X_{CH4}	ρ_{bulk}
1076	ThTOT↦V;$ThCO_2$↦L	0.831	0.141	0.011	0.614	0.327	0.055	0.004	0.741
Chirriato	"	0.823	0.152	0.012	0.613	0.324	0.059	0.004	0.740
	"	0.822	0.164	0.014	0.607	0.325	0.063	0.004	0.743
056	"	0.832	0.164	0.004	0.468	0.443	0.087	0.002	0.711
100m E-W	"	0.837	0.159	0.004	0.779	0.185	0.035	0.001	0.828
Vein	"	0.825	0.172	0.003	0.600	0.330	0.069	0.001	0.749
	ThTOT↦L;$ThCO_2$↦V	0.951	0.039	0.010	0.289	0.676	0.028	0.007	0.697
	"	0.952	0.035	0.013	0.612	0.370	0.013	0.005	0.768
001	"	0.941	0.049	0.010	0.750	0.236	0.012	0.002	0.821
Penon	ThTOT↦L;$ThCO_2$↦L	0.957	0.037	0.006	0.916	0.080	0.003	0.001	0.931
	ThTOT↦L;$ThCO_2$↦V	0.952	0.030	0.018	0.291	0.675	0.021	0.012	0.693
	ThTOT↦L;$ThCO_2$↦L	0.967	0.018	0.015	0.787	0.206	0.004	0.003	0.841
	ThTOT↦L;$ThCO_2$↦V	0.866	0.116	0.018	0.844	0.135	0.018	0.003	0.866
	ThTOT↦L;$ThCO_2$↦L	0.961	0.031	0.008	0.612	0.373	0.012	0.003	0.770
1014c	"	0.933	0.060	0.007	0.477	0.488	0.031	0.004	0.730
Barren Vein	"	0.960	0.029	0.011	0.786	0.205	0.006	0.002	0.841
Au<0.05ppm	"	0.957	0.038	0.005	0.845	0.148	0.006	0.001	0.878
	"	0.965	0.027	0.008	0.612	0.375	0.01	0.003	0.772
	"	0.952	0.049	0.001	0.608	0.372	0.019	0.000	0.772

and not the prograde metamorphic fluids. Mesothermal gold deposits commonly have a late-kinematic timing and formed from CO_2-rich fluids (Groves and Foster, 1991). One possible model is that at relatively shallow levels in the crust, the peak of metamorphism would be of a deeper-later type due to erosion (Powell *et al.*, 1991). The *P–T* evolution of the La Codosera area, determined by fluid inclusion studies, suggests that uplift and erosion occurred between peak metamorphism and the late-kinematic gold mineralisation. A consequence of this model is that fluids from rocks undergoing prograde metamorphism at depth would migrate to shallower crustal levels where metamorphic dehydration reactions had already terminated (Powell *et al.*,

op. cit.). Field evidence indicates that the majority of the mineralised veins lie along faults which connect to the Badajoz–Cordoba shear zone (Roberts *et al.*, 1991). The location of mineralisation is apparently controlled by fluid focusing along these major structures. Thus, Au could be mobilised by the prograde metamorphism at depth and nitrogen could be sourced either from metamorphic devolatisation reactions at depth or by fluid–rock interaction locally.

Conclusions

1. Pelite mineralogy, vitrinite data and fluid inclusion data from early fabric-parallel veins, constrain the peak metamorphism of the pelites to the upper greenschist facies with pressures of 1.4–3.1 kbar and temperatures of 325–425 °C.
2. Mineralisation occurs within late-kinematic post-peak metamorphism veins.
3. An unmixing low-salinity aqueo-carbonic fluid inclusion population indicates a *P–T* of formation for both the mineralised and barren late kinematic veins of 300 °C at 1.5 kbar.
4. A nitrogen anomaly is developed within the mineralised late-kinematic veins which results from fluid–rock interaction and reflects the channelling of the mineralising fluid along structures which have developed a connectivity to the Badajoz shear-zone.

Acknowledgements

This work was completed under the auspices of an EEC raw materials research grant No. MA1M-0032-C(A). S. J. Dee acknowledges receipt of a University of Southampton studentship. Dave Sanderson, Bob Foster and Jamie Wilkinson are thanked for their constructive reviews of the manuscript.

References

Arthaud, F. and Matte, P. (1975) Les décrochements tardi-Hercyniens du sud-ouest de l'Europe. Géométry et éssai de reconstitution des conditions de la deformation. *Tectonophysics*, **25**, 139–71.

Barker, C. E. and Pawlewicz, M. J. (1986) The correlation of vitrinite reflectance with maximum temperature in humic organic matter. In *Lecture Notes in Earth Sciences 5: Palaeogeothermics* (Buntebarth, G. and Stegena, L., eds.). Springer Verlag, Berlin, 79–93.

Bottrell, S. H., Shepherd, T. J., Yardley, B. W. D., and Dubessey, J. (1988*a*) A fluid inclusion model for the genesis of the Dolgellau gold belt, North Wales. *J. Geol. Soc.*, **145**, 139–45.

—— Car, L. P., and Dubessy, J. (1988*b*) A nitrogen rich metamorphic fluid and coexisting minerals in slates from North Wales. *Mineral. Mag.*, **52**, 451–7.

Bowers, T. S. and Helgeson, H. C. (1983*a*) Calculation of the thermodynamic and geochemical consequences of non-ideal mixing in the system H_2O–CO_2–NaCl on phase relations in geological systems: Equation of state for H_2O–CO_2–NaCl fluids at high temperatures and pressures. *Geochim. Cosmochim. Acta*, **47**, 1247–75.

Brown, P. E. (1989) FLINCOR: A fluid inclusion data reduction and exploration program. In PACROFI II. Programme with Abstracts, 14.

—— and Lamb, W. M. (1989) *P–V–T* properties of fluids in the system H_2O–CO_2–NaCl: New graphical presentations and implications for fluid inclusion studies. *Geochim. Cosmochim. Acta*, **53**, 1209–21.

Burg, J. P., Inglesias, M., Laurent, P. H., Matte, P. H., and Ribeiro, A. (1981) Variscan intercontinental deformation: the Coimbra Cordoba Shear Zone (SW Iberian Peninsula). *Tectonophysics*, **78**, 161–77.

Dubessy, J., Audeoud, D., Wilkins, R., and Kosztolanyi, C. (1982) The use of the Raman microprobe MOLE in the determination of the electrolytes dissolved in the aqueous phase of fluid inclusions. *Chem. Geol.*, **37**, 137–50.

Dee, S. J. (1992) *Tectonic controls and fluid evolution of auriferous quartz veins in the La Codosera area SW Spain*. Unpublished PhD. thesis, University of Southampton, U.K., 353 pp.

Duit, W., Jansen, J. B. H., Van Breemen, A., and Bos, A. (1986) Ammonium micas in metamorphic rocks as exemplified by Dome de L'Agout (France). *Am. J. Sci.*, **286**, 702–32.

Groves, D. I. and Foster, R. P. (1991) Archean Lode Gold Deposits. In *Gold metallogeny and Exploration*. (R. P. Foster, ed.), Blackie, London, 63–103.

Haendel, D., Mühle, K., Strühl, G., and Wand, U. (1979) Variationen der slickstoffisotopen in regionalmetamophen gesteinen: Zentralinstuit für Isotopen: *Stralenforsch. Mitt.*, **26**, 64–6.

Hallam, M. and Eugster, H. P. (1976) Ammonium silicate stability relations. *Contrib. Mineral. Petrol.*, **57**, 227–44.

Hoffman, J. and Hower, J. (1979) Clay mineral assemblages as low grade metamorphic geothermometers: application to the thrust faulted disturbed belt of Montana, U.S.A. In *Aspects of Diagenesis* (Scholle, P. A and Schluger, P. R., eds.). Spec. Publ. Soc. Econ. Pal. Min., **26**, 55–79.

Lefort, J. P. and Ribeiro, A. (1980) La faille Porto–Badajoz–Cordonne a-t-elle controllé l'évolution de l'ocean Paléozoique Sud Armorican. *Bull. Soc. Geol. Fr. 7. XXII.*, **3**, 455–62.

Naden, J. and Shepherd, T. J. (1991) Fluid inclusion volatiles and gold mineralisation in central Iberian granite and schist terranes. *Plinius*, **5**, 157.

Nesbitt, B. E. (1991) Phanerozoic Gold Deposits. In *Gold Metallogeny and Exploration* (R. P. Foster, ed.). Blackie, London, 104–32.

Nitsch, K. H. (1970) Experimentelle bestimmung der oderen stabilitatsgrange von stilpnomelam. (Abstract) *Fortsch. Mineral.*, **47**, 48–9.

Potter, R. W., Clynne, M. A., and Brown, D. L. (1978) Freezing point depression of aqueous sodium chloride solutions. *Econ. Geol.*, **73**, 284–5.

Powell, R., Will, T. M., and Phillips, G. N. (1991) Metamorphism in Archaean greenstone belts: calculated fluid compositions and implications for gold mineralisation. *J. Met. Geol.*, **9**, 141–50.

Price, L. C. (1983) Geologic time as a parameter in organic metamorphism and vitrinite reflectance as an absolute palaeogeothermometer. *J. Petrol Geol.*, **6**, 5–38.

Ramboz, C., Schnapper, D., and Dubessy. J. (1985) The P–V–T–X–f_{O_2} evolution of a H_2O–CO_2–CH_4 bearing fluid in a wolframite vein: Reconstruction from fluid inclusion studies. *Geochim. Cosmochim, Acta*, **49**, 205–19.

Roberts, S., Sanderson, D. J., Dee, S. J., and Gumiel, P. (1991) Controls on gold mineralisation in the La Codosera area, SW Spain. *Econ. Geol.*, **86**, 1012–22.

Sanderson, D. J., Roberts, S., McGowan, J. A., and Gumiel, P. (1991) Hercynian transpressional tectonics at the southern margin of the Central Iberian Zone, west Spain. *J. Geol. Soc. Lond.*, **148**, 893–8.

Seward, T. M. (1989) The hydrothermal chemistry of gold and its implications for ore formation: boiling and conductive cooling as examples. *Econ. Geol.* Monograph, **6**, 398–404.

Shepherd, T. J. (1981) Temperature programmable, heating–freezing stage for microthermometric analysis of fluid inclusions. Ibid., **76**, 1244–7.

—— Rankin, A. H., and Alderton, D. H. M. (1985) *A practical guide to fluid inclusion studies*. Blackie, London, 239 pp.

Wilkinson, J. J. (1991) Volatile production during contact metamorphism: the role of organic matter in pelites. *J. Geol. Soc.*, **148**, 731–6.

Zhang, Y. and Frantz, J. D. (1987) Determination of the homogenisation temperatures and densities of supercritical fluids in the system NaCl–KCl–$CaCl_2$–H_2O using synthetic fluid inclusions. *Chem. Geol.*, **64**, 335–50.

[*Manuscript received 1 September 1992: revised 19 February 1993*]